Dynamics of a supercooled polymer melt above the mode-coupling critical temperature: cage versus polymer-specific effects

2000 J. Phys.: Condens. Matter 12 6365

(http://iopscience.iop.org/0953-8984/12/29/308)

J. Phys.: Condens. Matter **12** (2000) 6365–6374. Printed in the UK PII: S0953-8984(00)11372-4

Dynamics of a supercooled polymer melt above the mode-coupling critical temperature: cage versus polymer-specific effects

J Baschnagel†‡§, C Bennemann†, W Paul† and K Binder†

† Institut für Physik, Johannes-Gutenberg Universität, 55099 Mainz, Germany
‡ Institut Charles Sadron, 6 rue Boussingault, 67083 Strasbourg, France

E-mail: baschnag@ics.u-strasbg.fr

Received 26 January 2000

Abstract. This paper reports results of molecular dynamics simulations for a glassy polymer melt consisting of short, non-entangled chains. The temperature region studied covers the supercooled state of the melt above the mode-coupling critical temperature. The analysis focuses on the interplay of simple-liquid and polymer-specific effects. One can clearly distinguish two regimes: a regime of small and one of large monomer displacements. The first regime corresponds to motion of a monomer in its local environment. It is dominated by the cage effect and well described by the idealized mode-coupling theory. The second regime is governed by the late-β/early-α process. In this regime the connectivity of the monomers begins to interfere with the cage dynamics and finally becomes dominant. The monomer displacement is compared with simulation results for a binary Lennard-Jones mixture to highlight the differences which are introduced by the connectivity of the particles.

1. Introduction

Bisphenol-A polycarbonate, atactic polystyrene, polybutadiene—three polymers with completely different chemical structure, but similar properties during the freezing process. They all undergo a glass transition. Due to the structural complexity, crystallization is effectively prevented or even *a priori* impossible. The polymer melts retain the high-temperature amorphous structure while the relaxation time increases by many orders of magnitude upon cooling towards the glass transition temperature T_g. These are typical features of the solidification process—not only for the three examples picked out above, but also for many other polymeric substances [1].

When trying to model the glassy freezing of polymer melts by computer simulations, an ideal choice would consist in studying a dense melt with a large number of long chains (chain length $N \sim 10^3$ to $N \sim 10^4$) while calculating the potentials from the simultaneous motion of nuclei and electrons (the Car–Parrinello method [2]). However, such a procedure is currently not feasible. The structural relaxation time of polymer melts with $N \geqslant 10^3$ is already at high temperatures of the order of milliseconds and larger, whereas the inclusion of the electrons' dynamics requires the time step of the simulation to be roughly 10^{-17} s. A disparity of at least 14 orders of magnitude in timescales cannot be covered in present day

§ Author to whom any correspondence should be addressed.

0953-8984/00/296365+10$30.00

simulations. Furthermore, the simultaneous simulation of electrons and nuclei also places a strong restriction on the size of the system. Typically, the number of particles simulated does not exceed one hundred.

Thus, introducing simplifications is necessary. There are several levels to this. First, the quantum-mechanical potential can be replaced by empirical potentials for the bond length, the bond angles, the torsional angles and the long-range interactions along the backbone of the chain. The latter interactions are typically modelled by a Lennard-Jones potential. After a judicious adaptation of the potential parameters an almost quantitative comparison with experimental data is possible. Such a comparison has been done for short chains of polyethylene [3] and polybutadiene [4] at high temperatures, for instance. However, reducing the temperature to the supercooled regime close to the mode-coupling critical temperature T_c [5] ($>T_g$) still represents a great challenge. On the other hand, this can be achieved by a further simplification of the model. The simplification consists in replacing the chains with chemical monomers and realistic potentials by chains of Lennard-Jones particles. This represents a minimal model for a polymer melt. The evolution of the slowing down of the structural relaxation when supercooling such a model is discussed in this paper.

2. A simple model for glassy polymer melts

This section compiles some properties of the model. A more detailed description can be found in references [6, 7].

2.1. Definition of the model

In the simulations, linear, monodisperse chains of length $N = 10$ (the non-entangled state) were used. All monomers interact by means of a truncated Lennard-Jones (LJ) potential,

$$U_{LJ}(r) = 4\epsilon[(\sigma/r)^{12} - (\sigma/r)^6] + C.$$

The constant $C = 0.007\,75$ shifts the potential such that it vanishes for $r \geqslant 2r_{min} = 2 \times 2^{1/6}\sigma$, where r_{min} is the minimum position. Temperature and distances are measured in units of ϵ/k_B and σ, respectively, and time is measured in units of $(m\sigma^2/\epsilon)^{1/2}$, where the mass is set to unity.

Furthermore, nearest-neighbour monomers along the backbone of a chain are bonded to each other by a FENE (finitely extensible non-linear elastic) potential,

$$U_F(r) = -15R_0^2 \ln[1 - (r/R_0)^2]$$

with $R_0 = 1.5$ [8]. With the parameters chosen, the superposition of the FENE and LJ potentials leads to a steep effective bond potential with a minimum at about 0.96σ (see figure 1).

The interplay of these potentials has two effects. First, the effective bond potential keeps neighbouring chain monomers so close together that bond crossings are impossible. Second, the favoured bond length of 0.96 is incompatible with r_{min}, and thus with crystalline ordering. By construction, the structure of the melt is therefore amorphous (see figure 2).

In summary, the polymer model used represents a variant of a (monatomic) Lennard-Jones model for simple liquids, in which crystallization is prevented by the competition between intrachain and interchain interactions.

2.2. Simulation procedure

In the simulations, a melt configuration contained 120 polymers of length $N = 10$. Ten independent configurations were simulated at each temperature to improve the statistics. The simulation procedure consisted of two steps. First, a simulation at constant pressure (mostly

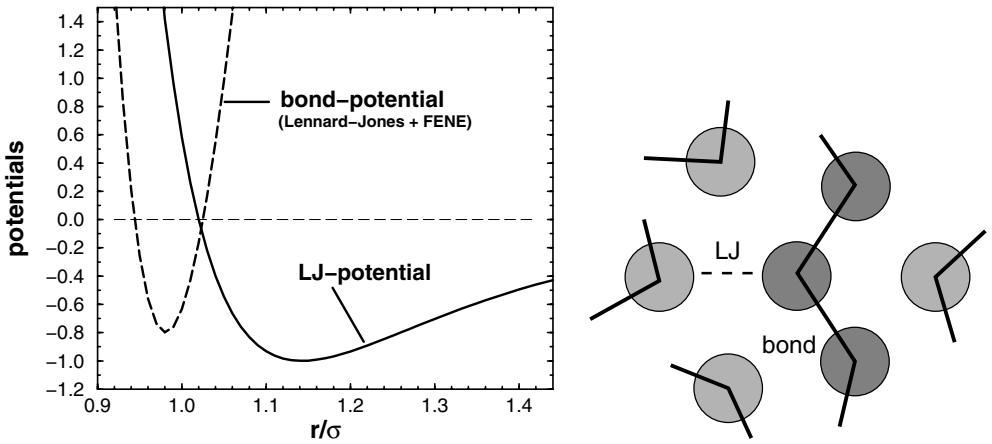

Figure 1. Effective bond (- - - -) and Lennard-Jones potentials (——). The bond potential results from a superposition of the Lennard-Jones and the FENE potentials and was shifted by -20 to put it on the same scale as the LJ potential (left-hand panel). The minimum position of the bond potential is smaller than that of the LJ potential. This incompatibility prevents the formation of a regular crystalline structure (right-hand panel).

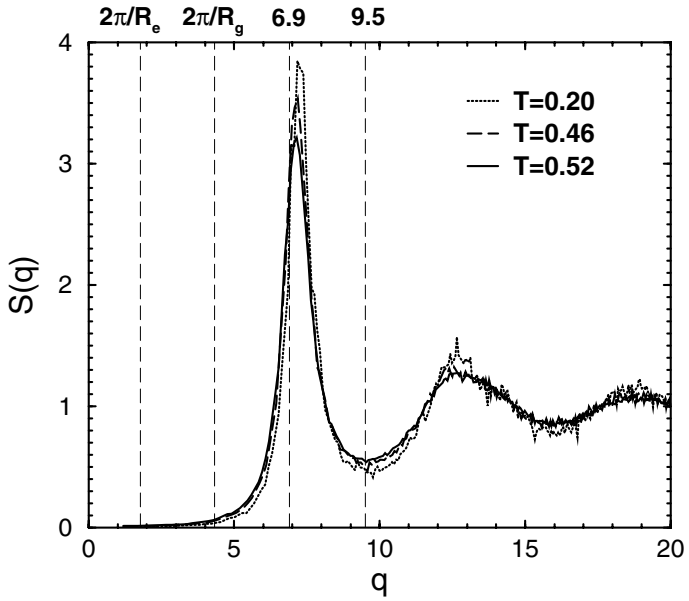

Figure 2. The temperature dependence of the melt's structure factor. The temperatures span the interval from the supercooled liquid ($T = 0.52$) to the glassy state ($T = 0.2$) of the melt. The mode-coupling critical temperature and the glass transition temperature are $T_c \simeq 0.45$ and $T_g \simeq 0.415$, respectively. In the mode-coupling analysis mostly $q = 3, 6.9, 9.5$ are used. The smallest q-value probes the size of a chain (end-to-end distance: $R_e \simeq 12.3$; radius of gyration: $R_g \simeq 2.09$), whereas the larger wave-vectors correspond to intermonomer distances.

$p = 1$) was carried out to find the density corresponding to this pressure and the desired temperature. The resulting volume was fixed, and then the simulation was continued in the canonical ensemble using the Nosé–Hoover thermostat. The dynamic properties of the model

are results from these canonical simulations. The first constant-pressure step was only used to equilibrate the melt at the given thermodynamic state point. Then, a second equilibration step was added in the canonical ensemble, in which each chain was propagated several times over the distance of the radius of gyration before starting the analysis. This time is sufficient for the incoherent scattering functions to have decayed to zero for all wave-vectors (except for $q < 2$ at $T = 0.46$).

2.3. Some static properties

The particular choice of the bonded and non-bonded potentials has two main consequences for the static properties of the model. First, the chains do not become stiffer with decreasing temperature. In the interesting temperature region ($T < 0.7$) the end-to-end distance, R_e, and the radius of gyration, R_g, are essentially constant: $R_e^2 \simeq 12.3$, $R_g^2 \simeq 2.09$. Second, there is no tendency to develop crystalline order. This is illustrated in figure 2 which shows the static structure factor $S(q)$ of the melt for $T = 0.2$, $T = 0.46$ and $T = 0.52$.

The lowest temperature is smaller than the best estimate of the model's glass transition, $T_g \simeq 0.415$, inferred from the temperature dependence of the specific volume during a (slow) quenching experiment [9]. The other temperatures are above the mode-coupling critical temperature (see section 3.1; best estimate $T_c \simeq 0.45$). In this relevant temperature range the structure factor remains essentially unchanged and exhibits the shape typical of an amorphous material.

3. Dynamics above T_c: simple-liquid versus polymer-specific effects

This section provides an overview of the dynamic properties of the model. It starts with a mode-coupling analysis [6, 10], which emphasizes the similarities of the melt studied to simple liquids, and then focuses on polymer-specific properties which become dominant in the diffusive regime [11].

3.1. Polymers as simple liquids: mode-coupling analysis

The key quantity of this analysis is the incoherent intermediate-scattering function

$$\phi_q^s(t) = \frac{1}{M}\sum_{m=1}^{M}\left\langle \exp\left(i\vec{q}\cdot[\vec{r}_m(t) - \vec{r}_m(0)]\right)\right\rangle \tag{1}$$

where $\vec{r}_m(t)$ denotes the position of the mth monomer at time t and M the total number of monomers. Figure 3 shows the typical decay of this correlation function for a temperature close to, but above T_c.

Initially, the scattering function decreases quickly. Since the monomer displacements are small at short times, this initial decrease can be well represented by a Gaussian approximation,

$$\phi_q^s(t) \simeq \exp\left[-\frac{1}{6}q^2 g_0(t)\right] \tag{2}$$

where $g_0(t)$ is the mean square displacement of all monomers. Equation (2) progressively deviates from the simulation data when the relaxation becomes retarded in an intermediate time interval. In this time interval, $\phi_q^s(t)$ is close to the non-ergodicity parameter f_q^{sc} [5]. The relaxation towards and away from f_q^{sc} occurs in two steps. This two-step relaxation can be fitted by the β-process of the idealized mode-coupling theory (MCT), which is (to leading order) given by [5, 12]

$$\phi_q^s(t) = f_q^{sc} + h_q^s G(t) \tag{3}$$

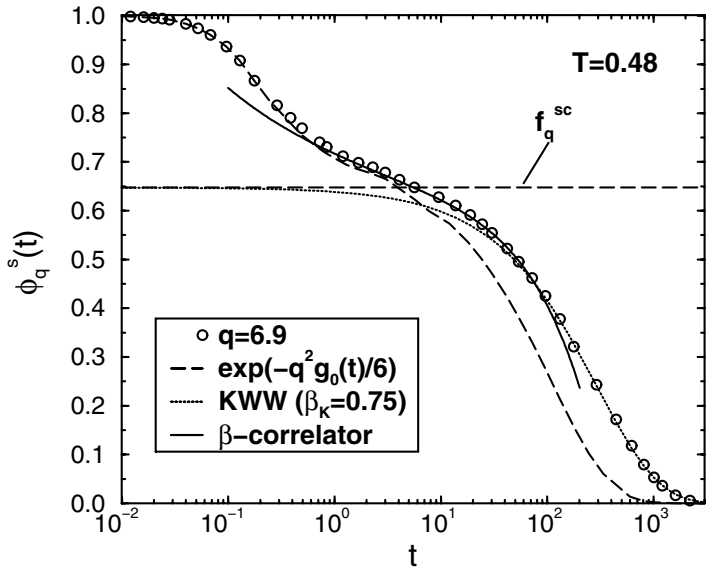

Figure 3. Comparison of $\phi_q^s(t)$ (○) for $T = 0.48$ and $q = 6.9$ ($\approx$ maximum of $S(q)$) with various theoretical approximations: a Gaussian approximation (equation (2)) (— — —), the MCT result for the β-regime (equation (3) plus corrections [12]) (——) and the Kohlrausch function (equation (4)) (· · · · · ·). The non-ergodicity parameter f_q^{sc} is indicated as a horizontal dashed line.

where $G(t)$ is the time- and temperature-dependent β-correlator and h_q^s a temperature-independent prefactor. The suggested physical picture underlying this formula is that particles in a liquid sit in 'cages' formed by their neighbours. At high temperatures, all particles are mobile. The cages open frequently due to fluctuations, and the enclosed particle can escape. However, as T_c is approached, the particles mutually block each other, which leads to a temporary slowing down of their motion. The signature of this 'cage effect' is the two-step process of $\phi_q^s(t)$ (and related correlation functions). Figure 3 shows that this picture developed for simple liquids is also applicable to the polymer melt studied. The second step represents the onset of the final structural relaxation, the α-process. A convenient description of the α-process is given by the Kohlrausch function

$$\phi_q^s(t) = f_q^{sc} \exp\left[-\left(\frac{t}{\tau_q}\right)^{\beta_q}\right] \tag{4}$$

where we fixed the amplitude to f_q^{sc} in the analysis [10]. This choice allows one to read off the relaxation time τ_q directly from the simulation data, so the exponent β_q is the only unknown parameter. In general, equation (4) is not a solution of the mode-coupling theory, except if $q \to \infty$ [13]. Then, β_q is identical to the von Schweidler exponent b which determines the onset of the α-process in mode-coupling theory [5]. For the present model, we found $\beta_q = b = 0.75$ already for $q \geqslant 3$.

3.1.1. Independence of the thermodynamic path. From the β-analysis, one obtains an estimate for the critical temperature, $T_c = 0.45$, and for the exponent $\gamma = 2.09$ which determines the divergence of the α-relaxation time in the idealized MCT:

$$\tau_q \sim (T - T_c)^{-\gamma}. \tag{5}$$

To test equation (5), we fixed $T_c = 0.45$ and determined γ for different q, and furthermore for different polymer-specific correlation functions which probe all length scales of a chain, ranging from the smallest one of a bond to the largest one of the end-to-end distance. The result is shown in figure 4.

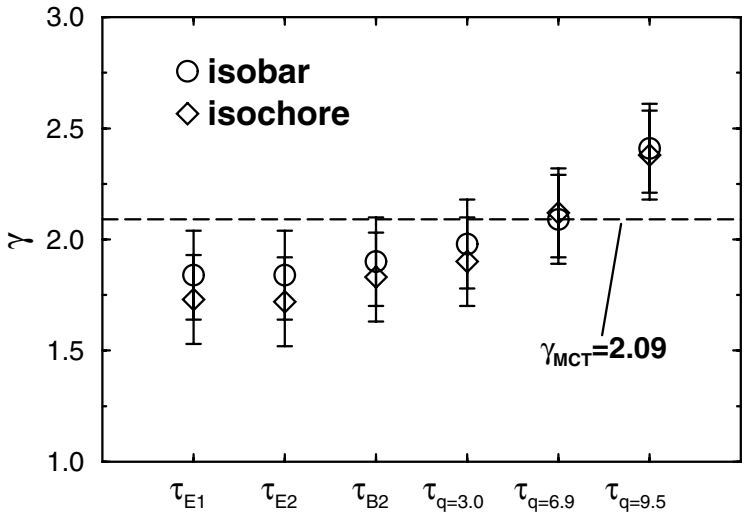

Figure 4. Values of γ, determined from the temperature dependence of various correlation times, for two different thermodynamic paths, which yield the same critical temperature. On the abscissa, the relaxation times are quoted, from which γ was determined: τ_{E1} = relaxation time of the first Legendre polynomial of the end-to-end vector, τ_{E2} = relaxation time of the second Legendre polynomial of the end-to-end vector, τ_{B1} = relaxation time of the first Legendre polynomial of the bond vector, τ_q = relaxation time of $\phi_q^s(t)$ for the respective q-value. For both the isobaric and the isochore path the error margins are about 10%, which is rather large, since γ is very sensitive to a variation of the critical temperature. Within the error bars, γ does not depend on the thermodynamic path. The prediction of the β-analysis, $\gamma = 2.09$, is shown as a horizontal dashed line. Taken from reference [7].

The γ-values obtained are close to the MCT result predicted from the β-analysis, but exhibit a systematic decrease when the length scale probed increases. On large length scales the tendency to freeze is less pronounced than locally. This observation is independent of the chosen thermodynamic path. Figure 4 compares results from an isobaric simulation at $p = 1$ with an isochoric simulation, in which the density was fixed at the value measured at $(T = T_c, p = 1)$. Therefore, the two simulations have the same critical point. Since MCT predicts that exponents, like γ, are thermodynamic quantities determined by $S(q)$ (and other thermodynamic properties) at T_c, the measured γ-value should be independent of the chosen path, if the paths have the same critical point. Figure 4 supports this prediction.

3.2. Escape from the cage: dominance of chain connectivity

The previous section emphasized the similarity between the polymer model studied and simple liquids. The connectivity of the monomers did not seem to have a dominant influence on the relaxation behaviour of the melt close to T_c. This is only true for the early β-process, and not for the escape from the cage, i.e., the onset of the α-process.

3.2.1. Mean square displacements. In order to illustrate the interplay of the cage effect and chain connectivity, figure 5 shows the mean square displacement of an inner monomer, $g_1(t)$, and of the chain's centre of mass, $g_3(t)$, again for $T = 0.48$ [11].

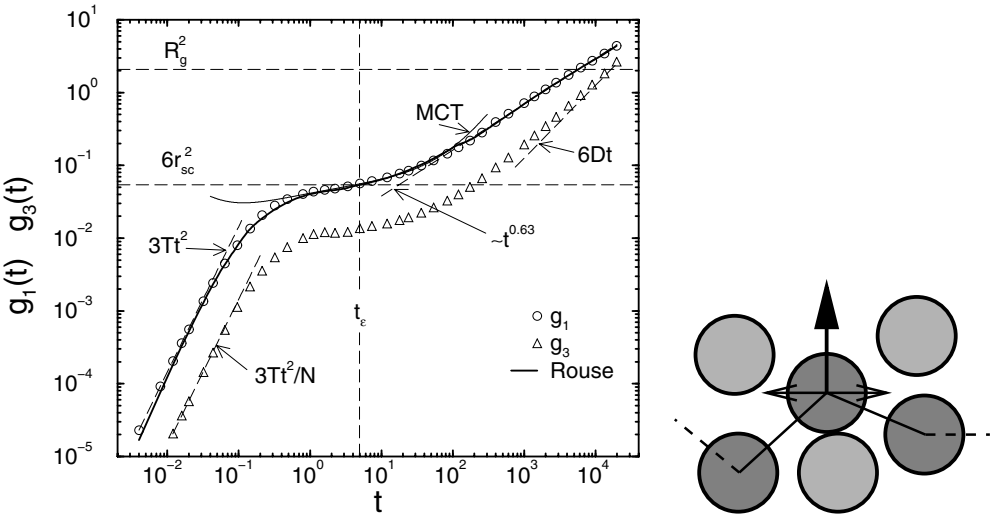

Figure 5. *Left-hand panel:* a log–log plot of the mean square displacements of an inner monomer, $g_1(t)$, and of the chains' centre of mass, $g_3(t)$, versus time for $T = 0.48$. The thick solid line is the Rouse formula for $g_1(t)$ (equation (6)). The initial ballistic behaviours for $g_1(t)$ and $g_3(t)$, i.e., $g_1(t) = \langle v^2\rangle t^2 = 3Tt^2$ and $g_3(t) = 3Tt^2/N$ ($\langle v^2\rangle$: mean square monomer velocity; $N = 10$: chain length), and the late-time diffusive behaviour are indicated as dashed lines. In addition, a power-law fit $g_1(t) \sim t^x$ with an effective exponent $x \simeq 0.63$ is shown as a thin solid line. The dashed horizontal lines represent the radius of gyration R_g^2 ($\simeq 2.09$; upper line) and the plateau value $6r_{sc}^2$ of the MCT analysis ($\simeq 0.054$; lower line), respectively. The dashed vertical line indicates the β-timescale t_ε. Additionally, the mode-coupling approximation in the β-relaxation regime is shown as a thin solid line. Taken from reference [11]. *Right-hand panel:* a schematic picture of the motion of a monomer in its cage. In the ballistic and early-β regime, the monomer performs a rattling motion in its local environment (indicated by $\longleftrightarrow$). Suppose that a 'hole' opens due to a fluctuation of the surrounding particles with the result that the monomer can move in the direction of the bold arrow. This does not necessarily lead to an escape from the cage because the monomer might be pulled back by the bonds to its neighbours, contrary to the behaviour in a simple liquid. Therefore, the α-process is dominated by chain connectivity, i.e., by polymer-specific effects.

At short times, the displacement of a monomer is so small that it does not feel surrounding monomers in the melt. The monomer moves freely, i.e., $g_1(t) \sim t^2$. At later times, this ballistic motion slows down due to the confinement imposed by its nearest neighbours. Over about two decades, $g_1(t)$ remains close to $r_{sc} \approx 0.095$, i.e., to a displacement that is about 10% of the monomer diameter. This is the regime of the β-relaxation, r_{sc} being the counterpart of f_q^{sc} in real space (see figure 3). Motions on this length scale are so small that the connectivity between the monomers does not significantly alter the dynamics of the polymer model studied compared to simple liquids [14]. This could be why mode-coupling theory can provide a reasonable explanation in the β-regime. However, as soon as the monomer tries to leave the cage, polymeric effects must become important. A particle in a simple liquid can always escape the cage, if a fluctuation opens a sufficient 'hole', whereas a monomer might be pulled back by the bonds to its neighbours. Therefore, there is another subdiffusive regime, $g_1(t) \sim t^{0.63}$, between the MCT β-process and free diffusion. This subdiffusive regime is visible for $g_1(t)$, but not for the mean square displacement of the centre of mass $g_3(t)$. The difference between

the two displacements results from the connectivity of monomers and can be understood quantitatively in terms of the (discrete) Rouse model (see figure 5):

$$g_1(t) = g_3(t) + 8\sum_{p=1}^{N-1}\langle|\vec{X}_p(0)|^2\rangle\Big[1-\Phi_p(t)\Big]\cos^2\left[\frac{(n-1/2)\,p\pi}{N}\right] \tag{6}$$

where $\Phi_p(t)$ is the relaxation function of the pth Rouse mode and $\langle|\vec{X}_p(0)|^2\rangle$ the corresponding normalization factor at $t = 0$. Equation (6) reflects the property that correlations between different modes, $p \neq q$, vanish (see the next paragraph). Further predictions of the Rouse model are: $\Phi_p(t) \propto \exp(-t/\tau_p)$ and $\langle|\vec{X}_p(0)|^2\rangle \propto p^{-2}$. On inserting these results in equation (6), one obtains $g_1(t) \sim t^{1/2}$ [15] instead of $g_1(t) \sim t^{0.63}$. This discrepancy suggests that the simulated Rouse modes exhibit a dependence on time and p different to that expected from theory.

3.2.2. Rouse modes. In a polymer melt, long-ranged excluded-volume and hydrodynamic interactions are screened [15]. For short, non-entangled chains the Rouse model is supposed to provide a good description of the polymer dynamics at high temperatures. The basic variables of the model are the normal modes of a chain, the Rouse modes. For the discrete polymer model studied, they are given by ($\vec{r}_n(t)$: position vector of the nth monomer)

$$\vec{X}_p(t) = \frac{1}{N}\sum_{n=1}^{N}\vec{r}_n(t)\cos\left[\frac{(n-1/2)\,p\pi}{N}\right] \qquad p = 0,\ldots,N-1. \tag{7}$$

The Rouse model predicts that the (normalized) correlation functions $\Phi_{pq}(t)$ for different modes p and q are orthogonal for all times, i.e., $\Phi_{pq}(t) \propto \delta_{pq}$, obey a time–temperature

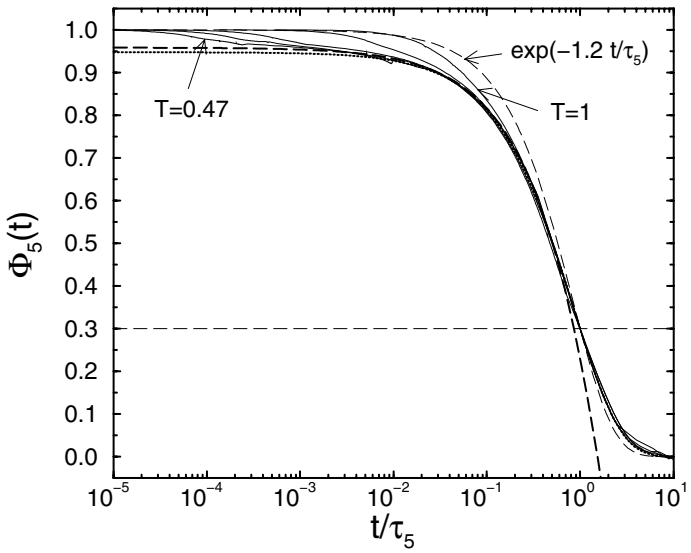

Figure 6. The correlation function of the fifth Rouse mode, $\Phi_5(t)$, versus the rescaled time t/τ_5 for five different temperatures: $T = 0.47$, 0.49, 0.52, 0.7, 1. The scaling time τ_5 is defined by $\Phi_5(\tau_5) = 0.3$ (dashed horizontal line). In addition, an exponential function (thin dashed line), a Kohlrausch function (dotted line) and a von Schweidler fit (thick dashed line) are shown. The Kohlrausch function is given by $0.948\exp[-1.15(t/\tau_5)^{0.87}]$ with $0 \leqslant \Phi_5(t) \leqslant 0.95$ as a fit interval. Using the von Schweidler exponent $b = 0.75$ from the mode-coupling β-analysis [10] and fitting $\Phi_5(t)$ for $10^{-4} \leqslant t \leqslant 0.5$, the result for the von Schweidler function is given by $0.959 - 0.815(t/\tau_5)^{0.75} + 0.086(t/\tau_5)^{1.5}$. Taken from reference [11].

superposition principle and decay exponentially. Whereas the first two predictions are realized by our polymer model, the relaxation is non-exponential already at high temperatures (see figure 6). Furthermore, time–temperature superposition is only observed for the final part of the relaxation. At intermediate times, $\Phi_p(t)$ exhibits a two-step relaxation. Therefore, the cage effect is also visible in this polymer-specific correlation function.

4. Summary

The main results of the present review can be summarized by a comparison of the dynamics of the polymer melt studied with a simple liquid. Figure 7 shows such a comparison. On plotting $g_1(t)$ for all temperatures as a function of time multiplied by the diffusion coefficient of the centre of mass at that temperature, we obtain the set of curves displayed in the inset of figure 7. The envelope of this set of curves is shown in the main part of the figure in comparison to the same master curve constructed for a binary Lennard-Jones fluid [16]. At large times the data for the two models have to agree by construction. At very early times the particles move freely, and both models exhibit ballistic motion, followed by the slow displacement of the MCT β-process. However, whereas the Lennard-Jones fluid directly crosses over from the cage effect to the free diffusion, the polymer exhibits the intervening connectivity-dominated

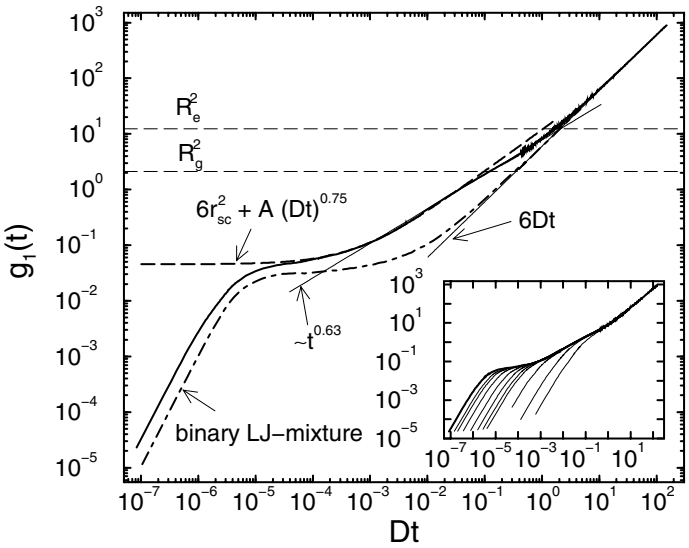

Figure 7. The master curve of the mean square displacement of an inner monomer $g_1(t)$ versus the rescaled time Dt (D: diffusion coefficient of a chain). The master curve (= thick solid line in the inset and the main figure) is constructed from the temperatures $T = 0.48, 0.49, 0.5, 0.52, 0.55, 0.6, 0.65, 0.7, 1, 2, 4$ (from left to right in the inset; the labels of the inset axes are identical to those of the main figure). The thick dash–dotted line is a master curve constructed from the simulation data for a binary Lennard-Jones mixture [16], including temperatures from $0.466 \leqslant T \leqslant 5$. Since $T_c \simeq 0.435$ for the binary mixture, but $T_c \simeq 0.45$ for the present polymer model, the lowest temperatures correspond to the same distance to the critical point, i.e., $T - T_c = 0.03$, in both cases. Additionally, two thin straight lines are shown, indicating a power-law fit to the monomer displacement, $g_1(t) \sim t^x$ with $x \simeq 0.63$, and the late-time diffusive behaviour $6Dt$ which is common to the simple liquid and the polymer data. The thick dashed line is a fit to an effective von Schweidler law (see the text). The dashed horizontal lines represent the end-to-end distance R_e^2 ($\simeq 12.3$; upper line) and the radius of gyration R_g^2 ($\simeq 2.09$; lower line), respectively.

regime for length scales between the bond length, $l \approx 1$, and the end-to-end distance R_e. In this regime the observed mean square displacement drops below the MCT description, which is here displayed as the effective von Schweidler law $6r_1^2 + A_1(Dt)^{0.75}$, with $r_1 = 0.087$ and $A_1 = 11.86$, before free diffusion finally sets in.

Acknowledgments

We are indebted to Drs W Kob, M Fuchs, I Alig, B Dünweg, A Latz, S C Glotzer for helpful discussions. In the course of this work, we have profited from generous grants of simulation time by the computer centre at the University of Mainz, the HLRZ Jülich and RHRK Kaiserslautern, which are gratefully acknowledged, as well as financial support by the Deutsche Forschungsgemeinschaft under SFB262/D2.

References

[1] McKenna G B 1989 *Comprehensive Polymer Science* vol II, ed C Booth and C Price (New York: Pergamon) pp 311–62
[2] Galli G and Pasquarello M 1993 *Computer Simulation in Chemical Physics* ed M P Allen and D J Tildesley (Dordrecht: Kluwer) pp 261–313
[3] Paul W, Smith G D, Yoon D Y, Farago B, Rathgeber S, Zirkel A, Willner L and Richter D 1998 *Phys. Rev. Lett.* **80** 2346
[4] Smith G D, Paul W, Monkenbusch M, Willner L, Richter D, Qiu X H and Ediger M D 1999 *Macromolecules* **32** 8857
[5] Götze W 1990 *Liquids, Freezing and the Glass Transition* part 1, ed J-P Hansen, D Levesque and J Zinn-Justin (Amsterdam: North-Holland) pp 287–503
[6] Bennemann C, Paul W, Binder K and Dünweg B 1998 *Phys. Rev.* E **57** 843
[7] Bennemann C, Paul W, Baschnagel J and Binder K 1998 *J. Phys.: Condens. Matter* **11** 2179
[8] Kremer K and Grest G S 1990 *J. Chem. Phys.* **92** 5057
[9] Binder K, Bennemann C, Baschnagel J and Paul W 1999 *Slow Dynamics in Complex Systems* ed M Tokuyama and I Oppenheim (Woodbury, NY: AIP Press) pp 193–204
[10] Bennemann C, Baschnagel J and Paul W 1999 *Eur. Phys. J.* B **10** 323
[11] Bennemann C, Paul W, Baschnagel J and Binder K 1999 *Comput. Theor. Polym. Sci.* **9** 217 (Bennemann C, Paul W, Baschnagel J and Binder K 1999 *Preprint* cond-mat/9902358)
[12] Fuchs M, Götze W and Mayr M R 1998 *Phys. Rev.* E **58** 3389
[13] Fuchs M 1994 *J. Non-Cryst. Solids* **172–174** 241
[14] Bennemann C, Donati C, Baschnagel J and Glotzer S C 1999 *Nature* **399** 246
[15] Doi M and Edwards S F 1986 *The Theory of Polymer Dynamics* (Oxford: Clarendon)
[16] Kob W and Andersen H C 1995 *Phys. Rev.* E **51** 4626